



HAL
open science

STEM observation of a multiphase nucleus of spheroidal graphite

Lydia Laffont, Alessandro Pugliara, Teresa Hungría, Jacques Lacaze

► **To cite this version:**

Lydia Laffont, Alessandro Pugliara, Teresa Hungría, Jacques Lacaze. STEM observation of a multiphase nucleus of spheroidal graphite. *Journal of Materials Research and Technology*, 2020, 9 (3), pp.4665-4671. 10.1016/j.jmrt.2020.02.093 . hal-02533969

HAL Id: hal-02533969

<https://hal.science/hal-02533969>

Submitted on 6 Apr 2020

HAL is a multi-disciplinary open access archive for the deposit and dissemination of scientific research documents, whether they are published or not. The documents may come from teaching and research institutions in France or abroad, or from public or private research centers.

L'archive ouverte pluridisciplinaire **HAL**, est destinée au dépôt et à la diffusion de documents scientifiques de niveau recherche, publiés ou non, émanant des établissements d'enseignement et de recherche français ou étrangers, des laboratoires publics ou privés.

Available online at www.sciencedirect.com

jmr&t
Journal of Materials Research and Technology
www.jmrt.com.br



Original Article

STEM observation of a multiphase nucleus of spheroidal graphite

Lydia Laffont^{a,*}, Alessandro Pugliara^{a,b}, Teresa Hungria^b, Jacques Lacaze^a

^a CIRIMAT, Université de Toulouse, BP 44362, 31030 Toulouse cedex 4, France

^b Centre de Microcaractérisation Raimond Castaing, Université de Toulouse, UPS – CNRS – INPT – INSA, 31400 Toulouse, France

ARTICLE INFO

Article history:

Received 10 February 2020

Accepted 27 February 2020

Available online xxx

Keywords:

Spheroidal graphite

Cast iron

Nucleus

Nitride

TEM

STEM-EDS

ABSTRACT

As part of a study on nucleation and growth of graphite in spheroidal graphite irons, systematic transmission electron microscopy observations are carried out. For this, focused ion beam is used to prepare thin foils that are precisely located and present an even thickness thus allowing high quality characterization.

In this work, a nucleus with an overall elongated shape that was found in a perfectly round graphite spheroid is investigated by scanning transmission electron microscopy (STEM) coupled with energy dispersive X-ray spectroscopy. The acquisition of STEM images at different tilt of this nucleus is achieved which allows illustrating the precipitation process of the many phases constituting it. For the first time, a remaining of inoculant could be identified within the nucleus. Furthermore, the elongated shape of the nucleus is a definitive proof that the shape of nucleus does not determine that of the emerging graphite precipitate.

© 2020 The Authors. Published by Elsevier B.V. This is an open access article under the CC BY-NC-ND license (<http://creativecommons.org/licenses/by-nc-nd/4.0/>).

1. Introduction

Spheroidal graphite cast irons are obtained by submitting a cast iron melt to a spheroidizing treatment (with Mg alone or with rare earths) followed by so-called post inoculation. These additions contain other elements which are mainly strong deoxidizers and/or desulfurizers. Accordingly, many of the observations made on graphite nuclei reported the presence of oxides, sulfides or oxysulfides. Some rationalization of these results has been proposed by Skaland et al. [1] who classified the particles acting as nuclei as A and B. Type A particles relate to a three-stage nucleation process consisting of precipitation of a sulfide on which forms an oxide on top of

which precipitates a complex oxide which is the actual nucleation substrate for graphite. Type B particles showed only the last two steps, i.e. they consist of a complex oxide on top of an oxide. Pan et al. [2] and Skaland et al. [1] stressed that the sulfide and the oxide were produced as a result of the spheroidizing treatment, meaning the sulfide contained Mg and Ca – or any other strong added desulfurizer – while the oxide was found to contain Mg and Si.

In contrast, Igarashi and Okada observed graphite nuclei consisting of a MgO core enveloped by MgS with sometimes the presence of small (Mg,Al,Si) nitrides at the periphery [3]. These authors noticed that the sulfide had often a rounded shape. This study was complemented by Nakae and Igarashi [4] who varied the amount of sulfur in a Mg-treated cast iron

* Corresponding author at: CIRIMAT, Université de Toulouse, CNRS, INPT, UPS, ENSIACET, 4 allée Emile Monso, BP 44362, 31030 Toulouse Cedex 4, France.

E-mail: lydia.laffont@ensiacet.fr (L. Laffont).

<https://doi.org/10.1016/j.jmrt.2020.02.093>

2238-7854/© 2020 The Authors. Published by Elsevier B.V. This is an open access article under the CC BY-NC-ND license (<http://creativecommons.org/licenses/by-nc-nd/4.0/>).

from 0.0022 wt.% to 0.083 wt.%. In all samples, a multiphase precipitation of nitride, sulfide and oxide could be observed at the graphite center but the phase considered as nucleus depended on the sulfur level. At very low sulfur content (0.0022 wt.%) this was a faceted nitride, at intermediate sulfur levels (0.0052 to 0.072 wt.%) a rounded (Mg,Ca) sulfide and at the highest sulfur level (0.083 wt.%) a faceted (Mg,Ca,Mn) sulfide. The rounded shape of the nucleus suggested it was liquid [3] or amorphous [4] at the time graphite precipitated onto it.

Though nitrides have been reported as possible graphite nuclei since a long time (see for example the review by Zhou Jiyang [5]), they have not always been considered and are not mentioned in the review by Harding et al. [6]. Thus, their quasi systematic appearance in the studies mentioned above appeared at first striking. Indeed, the type B Mg-Si bearing precipitates identified by Skaland et al. [1] were later indexed as nitrides by Solberg and Onsoien [7] who showed them to have a trigonal structure very close to the hexagonal structure of AlN. Interestingly, they were found to act as nuclei when the undercooling for solidification was increased by adding rare earths to the melt [8], though Solberg and Onsoien found a layer of oxide on top of the nitride in some cases. It is quite possible that this increased complexity in the description of the graphite nucleation mechanism has to do with the definitive improvements in energy dispersive X-ray spectroscopy (EDS) in the late 1990s.

That the nuclei appear multiphase in the examples presented above complicates the analysis of the sequence of phase transformations leading to the nucleus. This complexity is further demonstrated by the description made here of a nucleus of a graphite nodule observed in a cast iron manufactured by thin-wall casting. In the present work, we present for the first time the complete organization of the nucleus of a graphite precipitate at sub-nanometric scale. The morphology and the chemical composition of this nucleus was studied using scanning transmission electron microscopy coupled with EDS cartographies. Moreover, the structural identification of the different crystallographic phases which compose the nucleus are carried out by electron diffraction analyses.

2. Materials and methods

The investigated spheroidal graphite cast iron was spheroidized with magnesium using an Fe-Si-Mg alloy whose chemical composition has been reported in Table 1 and its final composition has been previously given [9], consisting mainly of 3.77 wt.% C and 1.9 wt.% Si, balance Fe. The melt was poured in a thin-wall casting in which a commercial Fe-Si inoculant (chemical composition done in Table 1) had been added. After casting, the material was graphitized by heat-treatment at 950 °C for 15 min.

A sample was then cut perpendicular to the casting surface and prepared by standard metallographic methods for observation with light microscopy and was also used to prepare a transmission electron microscopy (TEM) specimen. On this section, a nodule was selected and a thin foil was prepared using the focused ion beam-lift out technique in a FEI NanoLab HELIOS 600i focused ion beam (FIB) / scanning elec-

tron microscope (SEM). TEM imaging was performed using electron microscopes: a JEOL JEM 2100F operated at 200 kV equipped with an EDS analyser (Bruker SDD Xflash 5030) and a JEOL cold-FEG JEM-ARM200F operated at 200 kV equipped with a probe Cs corrector (resolution 0.78 Å) and a JEOL CENTURIO SDD EDS detector. Diffraction patterns were recorded using selected area electron diffraction (SAED) mode with a 150 nm aperture, a convergent-beam of 50 nm with a convergence semi-angle less than 0.01° or a digital diffraction pattern obtained by fast Fourier transform (FFT) of high resolution TEM (HRTEM) images. All the diffraction patterns were indexed using the diffraction pattern simulation obtained by JEMS program [10]. During TEM examination, care was taken for minimizing the time during which the beam was focused on the observed areas to avoid graphite amorphisation. This was particularly needed when electron diffraction patterns had to be recorded.

3. Results and discussion

Fig. 1a is a mosaic image made of bright field (BF) TEM micrographs of the thin foil prepared by FIB. The spheroid has a diameter of about 8 μm. Fig. 1b shows a close-up of one part of the spheroid on which the conical sectors radiating for the nodule center can be easily observed. Within one of the sectors, a high resolution image was acquired in location labelled 1 in Fig. 1b which is 1 μm away from the nucleus. This image is reported in Fig. 1c and clearly shows that the stacking of the graphite layers is highly regular. The FFT of the HRTEM image (insert in Fig. 1c) presents well-defined spots representing (0002) reflections and reveals that the graphite was highly crystalline with its c-axis roughly parallel to the spheroid radius. Finally, in Fig. 1d, the nucleus appears of being a composite object made of two parts, namely an elongated nearly rectangular tail loosely connected to a more rounded part.

Further investigation of this nucleus was performed by tilting the sample each 2° from -60° to +60° around its long axis as illustrated with six views in Fig. 2. For comparison, BF TEM and high-angle annular dark-field (HAADF) STEM images (inserts) have been acquired in each tilt position. While the connection between the graphite sectors and the nucleus can be followed in the BF TEM image, the nucleus chemical composition is emphasized with the HAADF STEM images. The BF TEM images clearly indicate that the radial structure of graphite starts from the nucleus. Moreover, this sequence evidences the faceted and geometric contours of the nucleus and the presence of a fan-like faceted precipitate in the round part. The HAADF STEM images reveal that the center of the round part is much brighter, and thus contains at least one element heavier than those present in the fan-like precipitate (Fig. 2d).

To more precisely characterize the chemical composition of the nucleus, STEM EDS analyses were performed. A HAADF STEM micrograph of the nucleus at tilt of 0° is presented in Fig. 3a. The elongated tail has an almost uniform grey contrast. The rounded part presents contrasts that indicate it is multi-phase. A fan-like faceted precipitate is seen to develop from the center, while the grey background may correspond to another phase. To study the chemical composition of this

Table 1 – Chemical composition (wt. %) of the spheroidization treatment and the inoculant.

	Fe	Si	Ce	La	Mg	Ca	Al	F	Mn	Zr
Fe-Si-Mg	Balance	45.52	0.487	0.492	7.75	1.13	0.858	–	0.224	–
Inoculant	12	57	–	–	<0.5	25	1	1.5	1	2

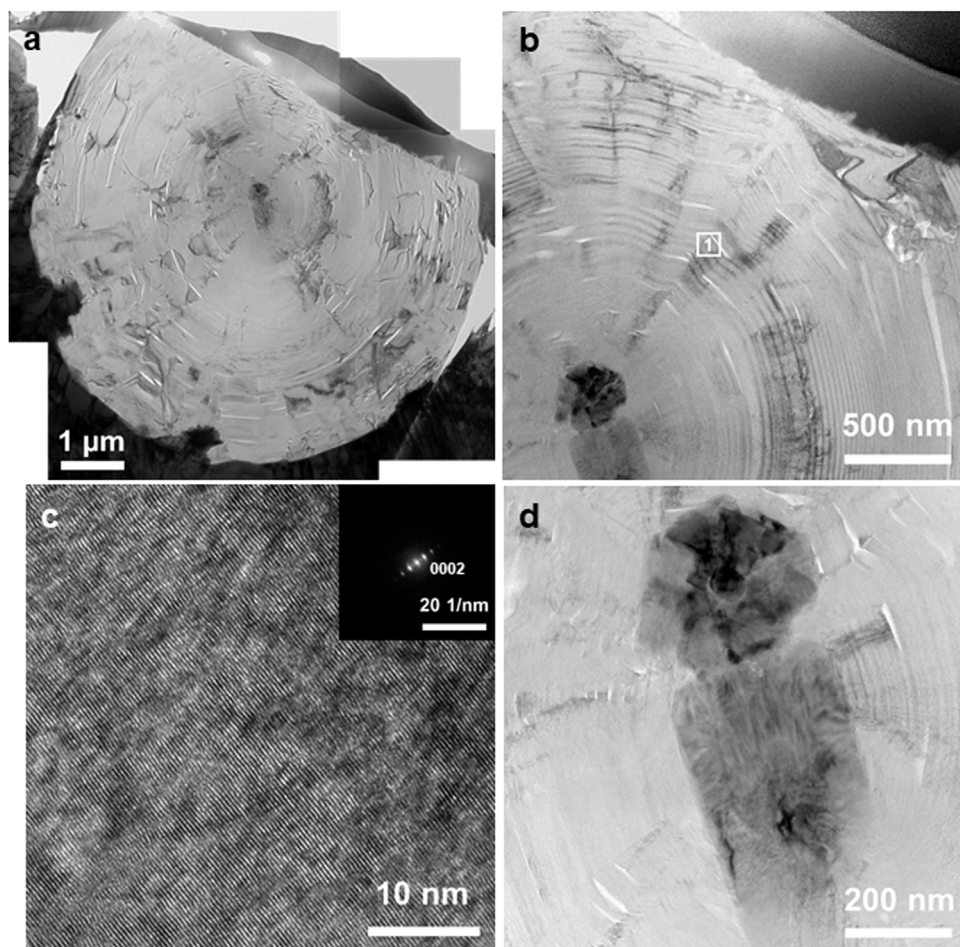


Fig. 1 – Mosaic image made of TEM bright field images of a graphite spheroid section (a) and close-up of the upper right part (b); high resolution image of the bulk graphite in location 1 in Fig. 1b with FFT (insert) of the image (c); BF image of the nucleus of the spheroid (d).

nucleus, EDS mappings of Al, Ti, Mg, Fe, Si, S and N elements have been acquired and are shown in Figs. 3b–h. The elongated phase is mostly composed of Al, Mg, Si and N, apart for some brighter spots which are rich in iron. Furthermore, these elements are also present in the rounded part of the nucleus but this rounded part consists of at least three more phases: the center rich in Fe, the shell around the center rich in S and the fan-like precipitate mostly composed of Ti.

Quantitative EDS analysis was performed by integrating the signal over small boxes labelled 1, 2 and 3 in Fig. 3a, and the results are listed in Table 2. It should be noted that only low levels of oxygen were detected. In this context, the grey contrast for the rounded and elongated parts have similar chemical composition and are composed of Mg, Al, Si and N. It could be noticed that EDS is not the most appropriate means for quantification of light elements as N and O and the error of these composition estimates may be important.

Table 2 – Chemical composition obtained by EDS in selected areas 1, 2 and 3 of Fig. 3a (at. %).

	Al	Mg	Si	N	O	S	Ti	Fe
1	16.3	32.5	39.9	10.3	2.4	0.9	0.3	0.5
2	14.2	29.3	32.9	20.5	1.6	1.1	0.1	0.4
3	15.4	31.7	35.6	11.3	4.1	1.6	0.3	0.0

For this phase, Mercier et al. [11] suggested a composition of 32 Si, 30 Mg, 4 Al and 34 N (in wt. %) and MgSiN_2 as a possible formula. Solberg and Onsoien [7] estimated the composition to 23.2 Si, 23.0 Mg, 6.9 Al and 46.9 N (at. %) and proposed to assign the formula $\text{AlMg}_{2.5}\text{Si}_{2.5}\text{N}_6$. Owing to the difficulties in measuring nitrogen content, Table 3 shows only the cation composition in at. % limited to the main elements, namely Al, Mg and Si for the two references cited above and our analyses. It can be seen that the Si contents are all very close to

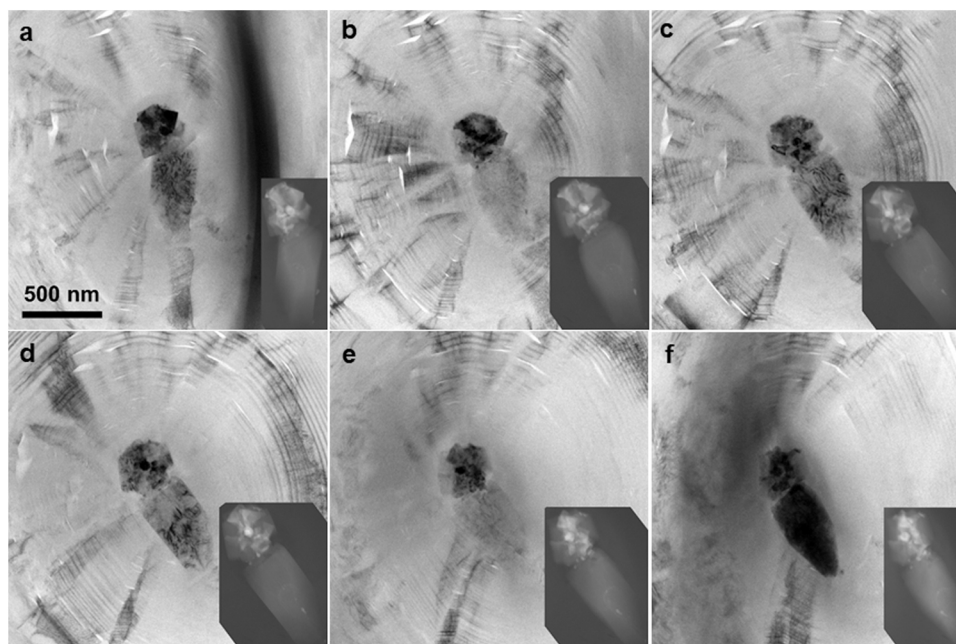


Fig. 2 – BF TEM images combined with HAADF STEM images (inserts) obtained with a tilt of -50° (a), -24° (b), -10° (c), $+6^\circ$ (d), $+24^\circ$ (e) and $+50^\circ$ (f).

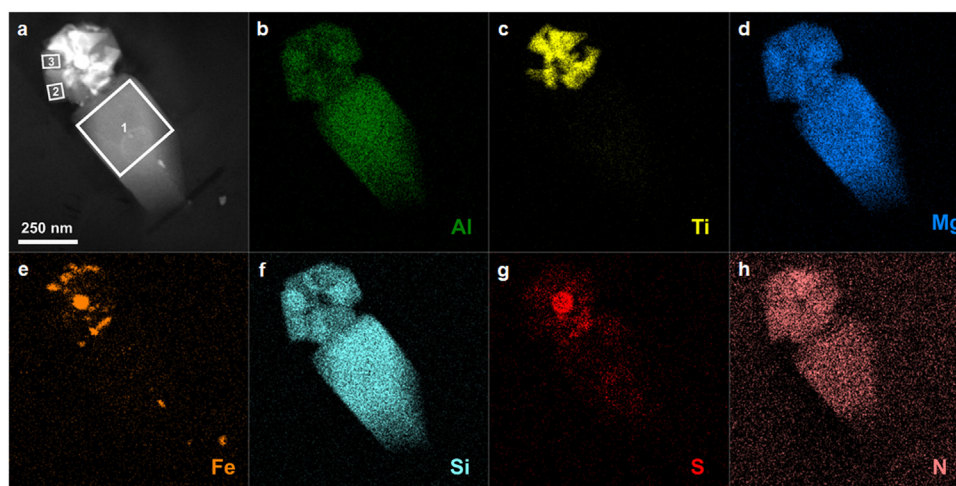


Fig. 3 – HAADF STEM image of the nucleus (a) and EDS mappings of Al, Ti, Mg, Fe, Si, S and N elements (b–h).

Table 3 – Cation composition (at. %) for the reported results as referenced in the column to the left.

	Al	Mg	Si
Mercier et al. [2]	5.9	49.0	45.1
Solberg and Onsoein [7]	13.0	43.3	43.7
This work, #1	19.0	37.9	43.1
This work, #2	18.6	38.3	43.1
This work, #3	18.7	38.3	43.0

each other while Al and Mg contents vary in opposite way suggesting a substitution of one by another.

A detailed chemical composition analysis was performed in the elongated tail. Fig. 4a shows a close-up of the STEM

HAADF image of the tail at tilt angle of 0° and Figs. 4a, 4b and 4c are the EDS mappings of Al, Mg and Si, respectively. Changes in composition are clearly seen which however could be related to changes in the foil thickness. In order to raise any doubt, line-scans were recorded in the long and transverse directions of the tail, which are numbered 1–3 in Fig. 4a. The line scan 1 (Fig. 4e) shows a chemical composition which corresponds perfectly to the measurements #1 (red dashed line in Fig. 4e–f) in Table 3. In contradistinction, the line scans 2 (Fig. 4f) and 3 (Fig. 4g) show that the Mg content decreases as the Al content increases while the silicon content is nearly constant. These results thus confirm that the changes in composition which appear in Figs. 4a–c are real and that Al and Mg can substi-

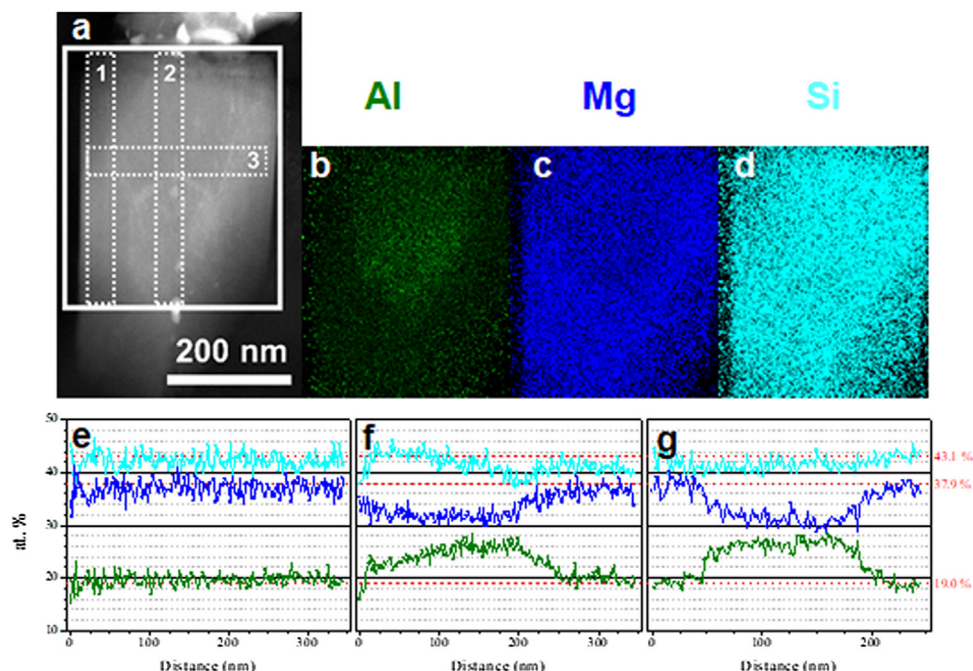


Fig. 4 – HAADF STEM image of the elongated part of the nucleus (a) and EDS mappings of Al (b), Mg (c) and Si (d) obtained from the white bold rectangle in a; EDS line-scans labelled 1 (e), 2 (f) and 3 (g) in (a) showing the change in content of the same three elements.

Table 4 – Chemical composition in selected areas of the round part of the nucleus of Fig. 5d (at. %).

	Al	Mg	Si	S	Ti	Fe
1	1.1	10.2	4.0	9.4	12.5	62.8
2	2.8	21.3	7.0	14.3	24.6	30.1
3	4.6	34.9	9.2	24.1	26.1	1.1
4	18.0	39.2	38.9	2.1	1.4	0.4
5	4.5	24.0	9.6	8.3	50.6	3.1

tute to each other. Accordingly, they suggest that the results in Table 3 from this work and literature could possibly represent the same phase.

To study the chemical composition of the multi-phase rounded part of the nucleus, focused STEM EDS analyses were carried out with a sub-nanometric probe. Figs. 5b and 5d show a superposition of the Fe (red), S (blue) and Ti (green) maps and the related HAADF STEM images shown in Figs. 5-a and 5-c respectively. Quantitative EDS analysis was performed by integrating the signal over small boxes labelled 1–5 in Fig. 5-d. The results are listed in Table 4.

These data are mainly indicative due to the overlapping of the different phases in each small box. Nitrogen has not been quantified in Table 4 due to the overlapping of Ti-L α and N-K α lines. Thus, in Fig. 5d, the center of the nucleus is probably iron-base phase (box 1) while the shell around is certainly a Mg-rich sulfide (boxes 2 and 3) which could possibly contain titanium. Further, the fan-like precipitate should be a titanium carbide or carbo-nitride (box 5) and the remaining area a (Al,Mg,Si) nitride (box 4). It should be noted that the iron phase in the center appears faceted (Fig. 5c) and that the fan-like precipitate seems to develop from the shell

around the iron center (Figs. 3a and 5a). Also noteworthy, Fe and S are detected between the rounded and elongated parts, and iron is also present at the outer border of the fan-like phase.

Finally, the foil and thus the different parts of the nucleus have been properly oriented for diffraction to have access to the crystallographic structure (see Fig. 6). Selected area electron diffraction (b) and convergent beam diffraction (d, f, h) were performed as illustrated in Fig. 6 with the related BF TEM images shown in the top row. The greyed area of Fig. 3a in both the elongated and rounded parts of the nucleus have been indexed as trigonal AlMg_{2.5}Si_{2.5}N₆ with a = b = 5.44 Å and c = 4.82 Å (space group, P31m) according to Solberg and Onsoien [7] (Figs. 6b and 6d). The fan-like precipitate can be indexed as cubic Ti(C,N)_{0.5} with a = 4.2822 Å (space group Fm-3m ICSD 618421 [12] (Fig. 6f) and the center of the nucleus as bcc-Fe (space group Im-3m - ICSD 631734 [13] (Fig. 6h). It was hardly possible to get information about the Mg-rich sulfide areas.

Though the most commonly reported nuclei are mixtures of oxides and sulfides, the literature shows that other types of phases may be encountered. In the present work, one single nucleus has been studied with modern analytical means which showed it, for the first time, to consist of at least four phases: 1) a center rich in Fe and indexed as bcc; 2) a sulfide rich in Mg; 3) a titanium carbo-nitride; 4) a nitride rich in Al, Mg and Si. From the spatial distribution of the phases, it seems that the above sorting corresponds also to the formation sequence of the nucleus: the Mg-rich sulfide is around the Fe-rich center; the Ti(C,N) fan-like precipitate develops from this sulfide; finally, the (Al,Mg,Si) nitride precipitates from all around this carbo-nitride. Moreover, it appears that the actual

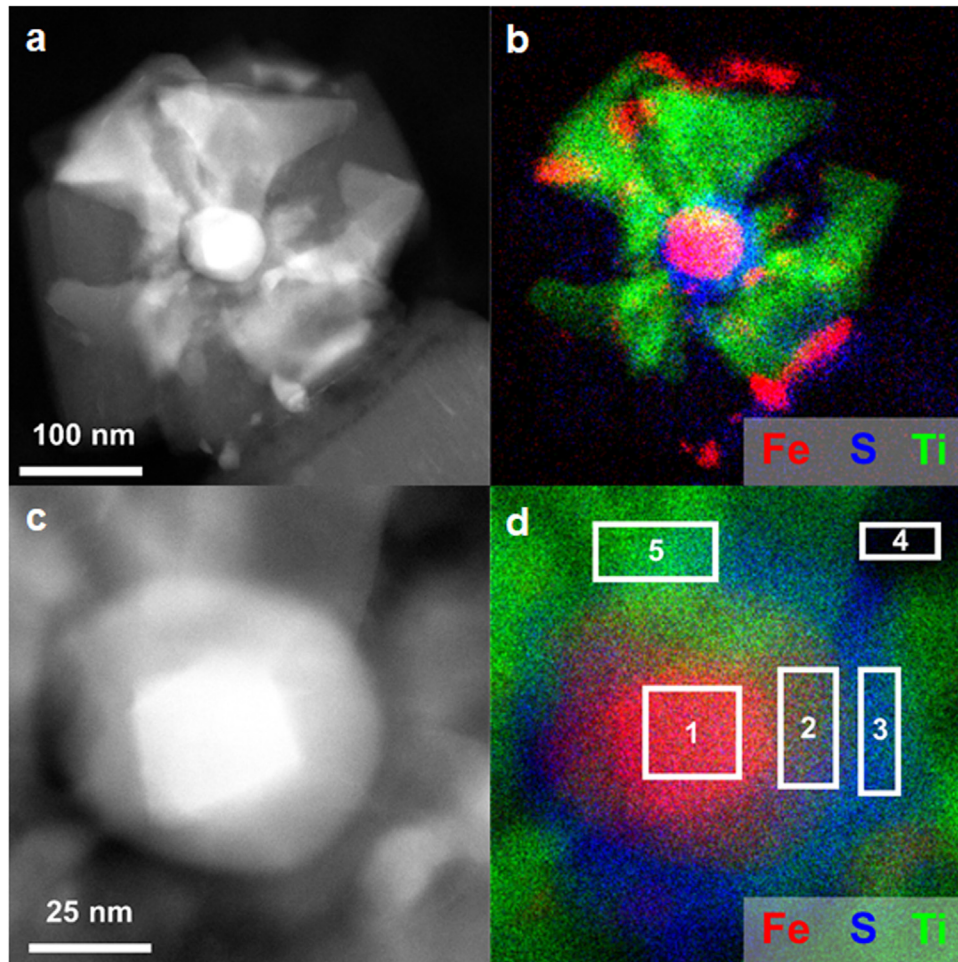


Fig. 5 – HAADF STEM images of the rounded part (a) and of the center (c) of the nucleus, and superimposition of EDS mappings of Fe (red), S (blue) and Ti (green) of the corresponding zones (b and d).

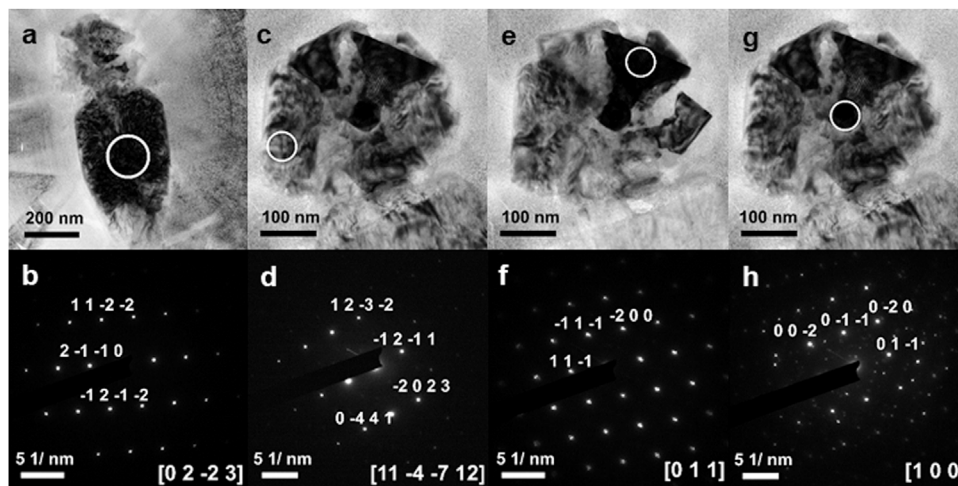


Fig. 6 – BF TEM images of the different parts of the nucleus (a, c, e and g) and associated electron diffractions (b, d, f and h).

substrate for graphite nucleation has been here the (Al,Mg,Si) nitride. This is at change with respect to the previous works showing nitrides [3,4] in that the inter-relation between the phases is here clearly seen.

The present results are also the first to report a Fe-rich bcc center which is guessed to be a remaining of the FeSi addition for inoculation. Furthermore, the elongated form of the nucleus is a definitive proof that the shape of a nucleus

does not determine that of the emerging graphite precipitate.

4. Conclusion

The use of modern analytical techniques combined with TEM allowed determining the phases that compose the nucleus of a graphite spheroid selected in a thin-wall cast-iron casting. The sequence of formation of this nucleus can be as follows: 1) a faceted center rich in Fe indexed as bcc which may be inherited from the inoculation process; 2) a shell around this center made of a sulfide rich in Mg; 3) then a fan-like titanium carbonitride developing from the shell; and finally 4) an nitride rich in Al, Mg and Si which precipitated both around the aggregate of the other phases and as a tail attached to this aggregate.

Conflicts of interest

The authors declare no conflicts of interest.

Data availability

The raw/processed data required to reproduce these findings cannot be shared at this time as the data also forms part of an ongoing study.

Appendix A. Supplementary data

Supplementary material related to this article can be found, in the online version, at doi:<https://doi.org/10.1016/j.jmrt.2020.02.093>.

REFERENCES

- [1] Skaland T, Grong O, Grong T. A model for the graphite formation in ductile cast iron: part I. Inoculation mechanisms. *Metall Trans A* 1993;24A:2321–45, <http://dx.doi.org/10.1007/BF02648605>.
- [2] Pan EN, Ogi K, Loper CR. *Analysis of the solidification of compacted/vermicular graphite cast iron*, 90. Chicago; USA: In: Transactions AFS Society, Proceedings of the 86th Annual Meeting; 1982. p. 509–27.
- [3] Igarashi Y, Okada S. Observation and analysis of the nucleus of the spheroidal graphite in magnesium-treated ductile iron. *IJCMR* 1998;11:83–8, <http://dx.doi.org/10.1080/13640461.1998.11819261>.
- [4] Nakae H, Igarashi Y. Influence of sulfur on heterogeneous nucleus of spheroidal graphite. *Mater Trans* 2002;43:2826–31, <http://dx.doi.org/10.2320/matertrans.43.2826>.
- [5] Jiyang Z. *Colour metallography of cast iron. Part 3, China Foundry* 2010;7:77–88.
- [6] Harding RA, Campbell J, Saunders NJ. *An assessment of our current understanding of the inoculation of cast iron. Rosemont, IL: In AFS International Inoculation Conference Proceedings; 1998.*
- [7] Solberg JK, Onsoien MI. Nuclei for heterogeneous formation of graphite spheroids in ductile cast iron. *Mater Sci Tech* 2001;17:1238–42, <http://dx.doi.org/10.1179/026708301101509313>.
- [8] Onsoien MI, Grong O, Skaland T, Jorgensen K. Mechanisms of graphite formation in ductile cast iron containing rare earth metals. *Mater Sci Tech* 1999;15:253–9, <http://dx.doi.org/10.1179/026708399101505815>.
- [9] Laffont L, Jday R, Lacaze J. An electron microscopy study of graphite growth in nodular cast irons. *Metall Mater Trans A* 2018;49A:1287–94, <http://dx.doi.org/10.1007/s11661-018-4508-4>.
- [10] Stadelmann P, JEMS-SWISS version 4.8130U2019b17, web site: <https://www.jems-swiss.ch/>.
- [11] Mercier JC, Paton R, Margerie JC, Mascré C. Inclusions dans les sphéroïdes de graphite. *Fonderie* 1969;277:191–200.
- [12] Alyamovskii SI, Mitrofanov BV, Zainulin Yu G, Shveikin GP. Coefficients of thermal expansion of titanium carbonitrides. *High Temp* 1973;11:616–61.
- [13] Straumanis ME, Kim DC. Lattice constants, thermal expansion coefficients, densities and perfection of structure of pure iron and of iron loaded with hydrogen. *Zeitschrift fur Metallkunde* 1969;60:272–7.

[1] Skaland T, Grong O, Grong T. A model for the graphite formation in ductile cast iron: part I. Inoculation